Available online at www.sciencedirect.com

ScienceDirect

Journal of the European Ceramic Society 34 (2014) 2095–2099

www.elsevier.com/locate/jeurceramsoc

Growth and luminescent properties of Ce-doped LiF/$LiLuF_4$ eutectic fibers grown by micro-pulling-down method

Yuui Yokota [a,*], Shunsuke Kurosawa [a,b], Kei Nishimoto [a], Valery Chani [b], Akira Yoshikawa [a,b]

[a] *Institute for Materials Research, Tohoku University, 2-1-1, Katahira, Aoba-ku, Sendai 980-8577, Japan*

[b] *New Industry Creation Hatchery Center (NICHe), Tohoku University, 6-6-10, Aoba, Aramaki, Aoba-ku, Sendai 980-8579, Japan*

Available online 22 January 2014

Abstract

The undoped and Ce-doped LiF/$LiLuF_4$ eutectic fibers with various ratios of LuF_3 to LiF were grown by the micro-pulling-down method for their application as neutron scintillators with light guiding structure. The differential thermal analysis (DTA) of undoped eutectic materials indicated that the eutectic point of LiF/$LiLuF_4$ was positioned around LiF 80 mol%–LuF_3 20 mol% composition. Some of the as-produced eutectic solids had rod-like regular array structures. This was observed using SEM images of cross-sectional and parallel cuts of the grown solids. In the range of $x \geq 0.28$, the dendrites appeared between the eutectic areas. Ce doped LiF/$LiLuF_4$ eutectic fibers demonstrated two emission peaks around 310 and 326 nm in the photoluminescence spectrum, and the decay time of the emission at 326 nm was 32.3 ns.

Keywords: Scintillator; Eutectic fibers; Micro-pulling-down method; $LiLuF_4$; Neutron

1. Introduction

Development of next-generation scintillating materials with high light yield and energy and spatial resolutions that can be used for radiation detection such as X-ray computer tomography (CT), homeland security, Positron Emission Tomography and others is always desired. Novel available materials include gadolinium oxy-sulfide (GOS), Gd_2O_2S arrays[1] and Tl-doped needle-structured cesium iodide (CsI).[2] However, spatial resolution of the detectors produced using these materials is not sufficient due to the structures that are not suitable for the proper optical wave guidance. Recently, eutectic materials composed of scintillator with rod-like (columnar) structure and the surrounding substance with higher refractive index have been developed.[3] For example, CsI-NaCl eutectic material had the phase-separated structure that was composed of columnar NaCl in the CsI matrix. Line profile of the spot-excited images for the Tl-doped CsI-NaCl eutectics indicated great light-guiding efficiency. Incoming Gamma-rays generated the scintillation light in the scintillating phase including activators. Thereafter, the scintillation light was transported to the surface of the eutectic scintillators with total reflection at the interface between scintillator and the matrix phases. The light-guiding system in the eutectic scintillators can improve the spatial resolution of radiation image. Thus, the spatial resolution of eutectic scintillators was over ten times greater than that of the present scintillators.

There are many previous reports about eutectic oxide materials fabricated by the micro-pulling-down (μ-PD) method including $Al_2O_3/RE_3Al_5O_{12}$ eutectic fibers that are substances with exceptional mechanical performance up to very high temperature.[4,5] The μ-PD crystal growth and/or solidification system is composed of custom-made crucible, high-frequency induction coil, insulators and a seed. This method has several advantages compared to conventional crystal growth techniques such as Czochralski (Cz) and Bridgeman–Stockbarger (BS) methods. One of the features of the μ-PD is its ability to produce crystal of fiber, columnar, plate, tube and other shapes depending on the crucible design.[6] In addition, high temperature gradient can be established at the solid–liquid interface during the crystal growth. This enables growth of the single crystals with approximately ten times greater growth rate compared to the conventional methods. Therefore, the μ-PD method is often used for novel crystal/material research.[7,8] In this communication, novel eutectic scintillating materials produced by the μ-PD method and having light guiding structure are reported.

$LiLuF_4$ fluoride crystal with the scheelite structure is a well known scintillating material for neutron detection.[9] In

* Corresponding author at: 2-1-1, Katahira, Aoba ku, Sendai 980 8577, Japan. Tel.: +81 22 215 2214; fax: +81 22 215 2215.
E-mail address: yokota@imr.tohoku.ac.jp (Y. Yokota).

0955-2219/$ – see front matter © 2014 Elsevier Ltd. All rights reserved.
http://dx.doi.org/10.1016/j.jeurceramsoc.2013.12.047

this crystal, Lu site can be substituted by rare-earth ions of Ce^{3+} and Nd^{3+} as emission centers, and Ce-doped $LiLuF_4$ (Ce:$LiLuF_4$) demonstrates relatively good scintillating properties. The phase diagram of the LiF–LuF_3 system has eutectic point of LiF/$LiLuF_4$ reported in the past.[10–12] According to the previous reports, this eutectic point corresponds to LiF/LuF_3 molecular ratio 80:20 and/or 78:22. Moreover, formation of rod-like structures in these eutectics was also observed.

This report deals with growth of undoped and Ce-doped LiF/$LiLuF_4$ eutectic materials by the μ-PD method and spatial distribution and configuration of the LiF and $LiLuF_4$ phases. In addition, formation of the optical guiding structures for the application in neutron scintillators and luminescent properties of these substances are discussed in some details.

2. Experimental

Undoped and Ce-doped $(1-x)$LiF–$x$$LuF_3$ eutectic materials were solidified using μ-PD method from melts of the following nominal compositions: $x = 0.2$, 0.22, 0.24, 0.26, 0.28, 0.3 and $(1-x)$LiF-$x$$(Lu_{0.995}Ce_{0.005})F_3$ $x = 0.28$. Starting materials, LiF, LuF_3, and CeF_3 (>4 N, Stella Chemifa Corp.) were mixed together and placed into a carbon crucible. The bottom of the crucible had an outlet (hole) of 2 mm in diameter. The crucible was heated to 200–300 °C using high-frequency induction coil in the chamber that was under high vacuum of approximately $\sim 10^{-4}$ Pa. This baking process was necessary to remove the moisture that was adhered by the surface of the powder particles, the crucible, fragments of thermal insulation unit, and interior surfaces of the chamber. Thereafter, high-purity Ar/CF_4 gas mixture (Ar:CF_4 = 9:1) was injected into the chamber. Then, the crucible was heated up to the melting point of the starting mixture. After the melting, the mixtures were solidified and cooled down to room temperature. These solids were used for the directional solidification of the eutectic mixtures by the μ-PD method and for the differential thermal analysis (DTA) measurements using SETSYS Evolution24 (SETARAM). The DTA data was necessary for the detailed study of the phase diagram around the eutectic point of LiF/$LiLuF_4$. The fluorides crystal growth by the μ-PD method is described in Ref. 7. The materials outlined here were solidified at pulling-down rate of 0.5 mm/min using Pt wire as a seed. The as-grown eutectic solids were cut and polished for the measurements, observations, and characterization of luminescent properties.

DTA measurements were performed around the eutectic point using pre-melted samples with various LuF_3: LiF ratios. The DTA curves were measured for the specimens placed in carbon crucibles in Ar atmosphere at 4 °C/min sweep rate. The phases of the solidified eutectic materials were identified by the X-ray diffraction (XRD) method. The local surface of the polished samples was observed with the scanning electron microscope (SEM) using back-scattered electrons (BSE). The chemical composition of the fragments of the local surface images was measured by the energy dispersive X-ray spectroscopy (EDX) combined with SEM. EDX mapping images were obtained using Lu K_α-line. Photoluminescence spectrum and the decay curve of the Ce-doped eutectic solid were measured using spectrofluorometer (FLS92 from Edinburgh Instruments) under ultraviolet excitation. The measured spectra were not spectrally corrected from instrumental response. Xenon lamp was used as an excitation source in the photoluminescence measurement and the decay curve at 326 nm was measured under 295 nm excitation.

3. Results and discussions

The DTA curves associated with the cooling process indicated exothermic peaks around 680 °C for all the samples as it is illustrated in Fig. 1(a). According to the previous reports, the peaks are attributable to the eutectic temperature. In the temperature range of 710–760 °C, an exothermal shoulder was observed

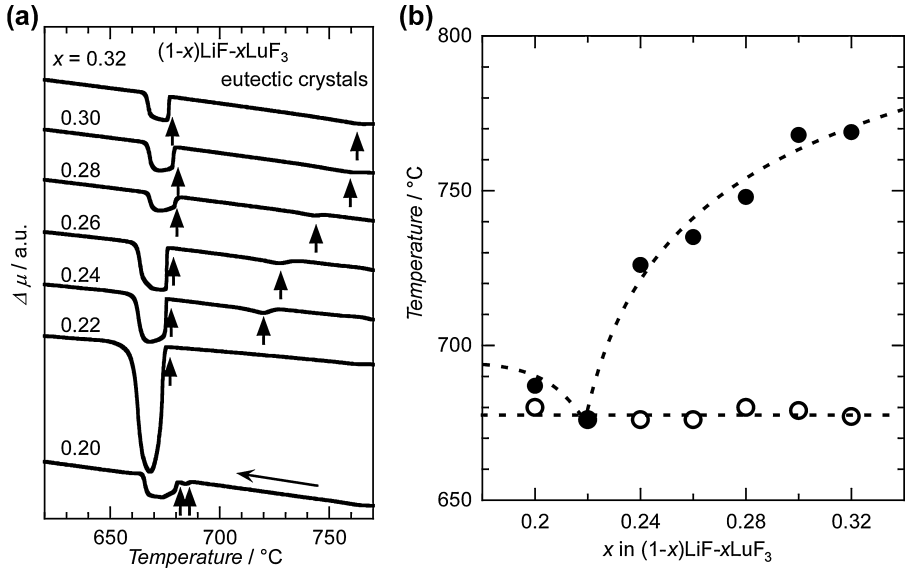

Fig. 1. (a) DTA curves of the LiF/$LiLuF_4$ eutectic materials with various x. (b) Fragment of the phase diagram around LiF/$LiLuF_4$ eutectic composition.

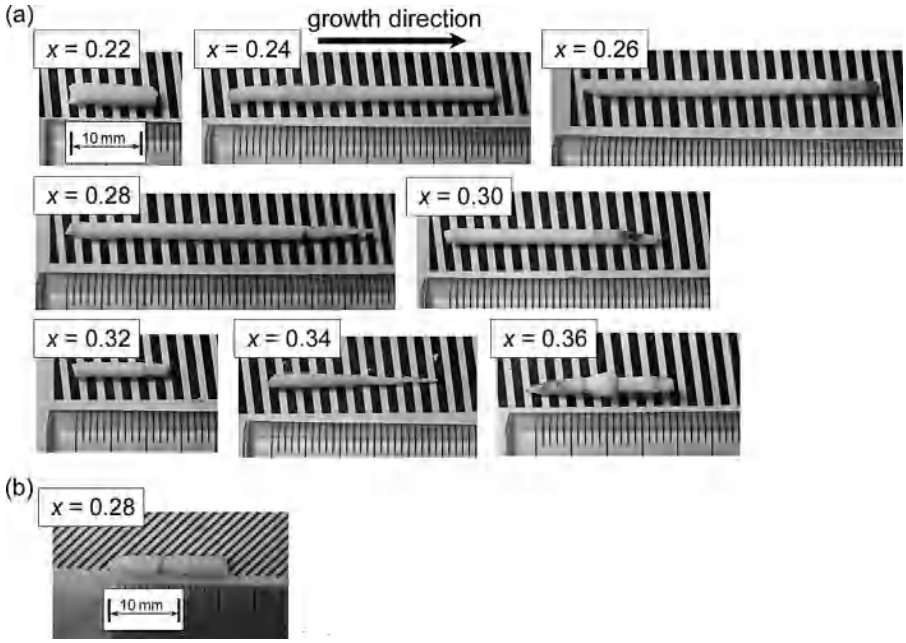

Fig. 2. (a) Undoped and (b) Ce-doped LiF/$LiLuF_4$ eutectic composites with various x in $(1-x)$LiF-$x$$LuF_3$.

in all the curves, and the temperature varied depending on x, suggesting that the related temperatures were the liquidus temperatures for the corresponding compositions. The eutectic and melting temperatures measurements results are summarized in the phase diagram (Fig. 1(b)). According to the phase diagram, the eutectic point observed in the LiF/$LiLuF_4$ system corresponded to the composition of 78 mol%LiF + 22 mol%LuF_3, or $x = 0.22$.

Undoped LiF/$LiLuF_4$ eutectic solids with various x were produced by the μ-PD method. During solidification, the liquid–solid interface was limited by the ϕ2 mm outlet of crucible. Therefore, the produced solids had shape of cylinders of approximately 2 mm in diameter. They had length of several centimeters along the solidification direction as it is demonstrated in Fig. 2(a). However, in the case of $x = 0.34$ and 0.36, the solid–liquid interface during solidification was unstable. As a result, diameters of these solids were not constant. In addition, Ce0.5% doped LiF/$LiLuF_4$ eutectic solid with $x = 0.28$ was grown (Fig. 2(b)).

Powder XRD patterns of undoped and Ce-doped eutectic solids with various x were examined to identify the phases, and the results are illustrated in Fig. 3. According to Fig. 3(a), all the diffraction peaks detected for the undoped solids were identified as those corresponding to the $LiLuF_4$ and LiF structures, and other phases were not found. The angles of the diffraction peaks for undoped eutectic materials were independent of

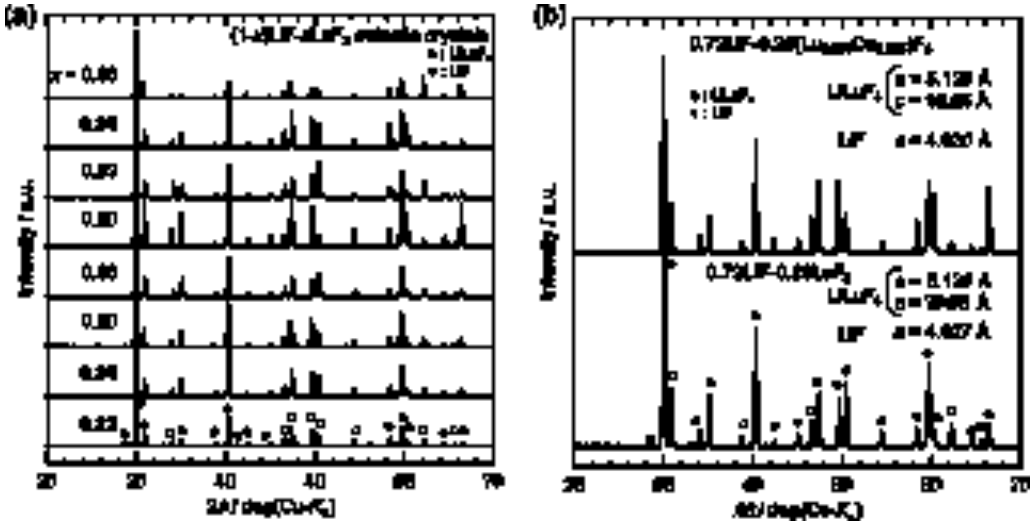

Fig. 3. Powder XRD patterns of the LiF/$LiLuF_4$ eutectic solids. (a) Undoped solids and (b) undoped and Ce-doped solids with $x = 0.28$.

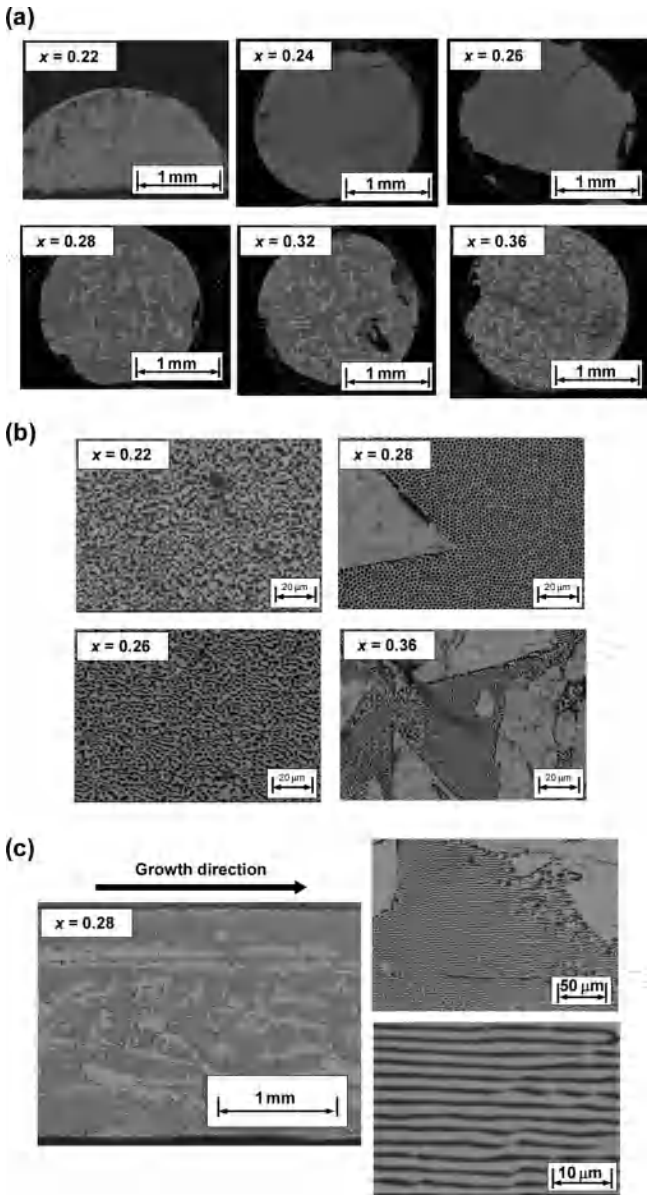

Fig. 4. SEM (BSE) images of cross-sectional cuts of undoped LiF/$LiLuF_4$ eutectic solids. (a) Whole and (b) enlarged images. (c) SEM (BSE) images of parallel cuts of undoped eutectic solids.

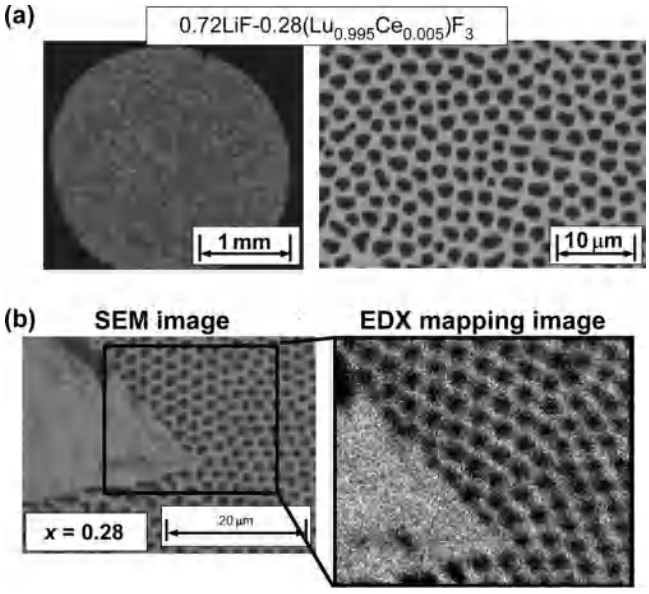

Fig. 5. (a) SEM (BSE) images of cross-sectional cuts of Ce-doped LiF/$LiLuF_4$ eutectic composite. (b) EDX mapping image produced using Lu-L_α-line.

x while the intensities of the diffraction peaks changed with increasing x. The relative intensities of the diffraction peaks corresponding to the $LiLuF_4$ phase systematically increased with increase of x compared to the peaks originated from the LiF phase. The Ce-doped eutectic solid was also formed by exclusively two phases of LiF and $LiLuF_4$ (Fig. 3(b)). The lattice parameters of the $LiLuF_4$ and LiF phases for undoped and Ce-doped solids with $x = 0.28$ were also calculated from the powder XRD patterns. a and c-axes lengths of the $LiLuF_4$ phase and a-axis lengths of the LiF phase did not demonstrate considerable variations.

The SEM images of the cross-sectional cuts of undoped eutectic solids produced using BSE are shown in Fig. 4. In the range of $x \geq 0.28$, the cluster phases with the dendrite structure appeared in the whole images (Fig. 4(a)), and the dendrites increased with increasing x. On the other hand, uniform areas with the eutectic structures were observed in the enlarged images of the samples with $x \leq 0.28$ (Fig. 4(b)). Moreover, the image of the sample with $x \geq 0.28$ contains uniform eutectic areas that are composed of rod-like phases sited in the matrix surrounding. According to Fig. 4(c) illustrating SEM images of the parallel cuts of undoped eutectic solids with $x = 0.28$, the dendrites grew along the growth direction. In addition, the eutectic areas with the rod-like structures oriented along the growth direction were observed between the dendrites. This is consistent with the previous report.[11] According to Fig. 5(a), the Ce-doped LiF/$LiLuF_4$ eutectic solids also demonstrated the eutectic areas with the rod-like structures and dendrites. The EDX mapping using Lu-L_α line indicated that rod-like phase was composed of LiF (Fig. 5(b)). Meanwhile, the matrix and dendrites were composed of $LiLuF_4$. The $LiLuF_4$ dendrites are considered to be generated from the excess $LiLuF_4$. Unfortunately, presence of the Ce^{3+} ions was not observed because concentration of Ce^{3+} was less than limit of detection in the EDX measurements. Most probably, Ce ions substituted for Lu site in the $LiLuF_4$ structure.

Fig. 6 demonstrates photoluminescence spectrum and the decay curve of the Ce-doped LiF/$LiLuF_4$ eutectic solid recorded under ultraviolet excitation. In the photoluminescence spectrum (Fig. 6(a)), two emission peaks around 310 and 326 nm were observed. These emissions are attributable to the 5d–4f transition of Ce^{3+} ion and the spectrum shapes of these emissions were consistent with that of Ce-doped $LiLuF_4$ single crystal.[13] Fig. 6(b) is the decay curve of the emission at 326 nm under 295 nm excitation. This curve was fitted by the single exponential function. The fitting curve and equation were described in Fig. 6(b). According to the fitting, the decay time was 32.3 ns, and it is considered to originate from 5d–4f transition of Ce^{3+} ion.

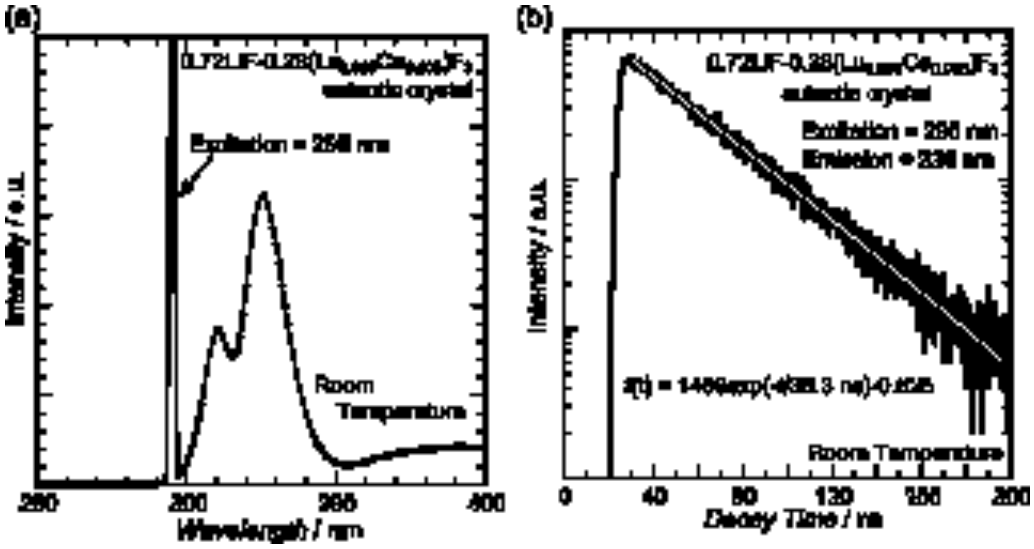

Fig. 6. (a) Photoluminescence spectrum and (b) decay curve of the Ce-doped LiF/$LiLuF_4$ eutectic composite.

4. Conclusions

The undoped and Ce-doped LiF/$LiLuF_4$ eutectic composites with various ratios of LuF_3 to LiF were produced by the μ-PD method, and their eutectic structures and luminescent properties were inspected. DTA curves for the cooling process indicated presence of the exothermic peaks around 680 °C corresponding to the eutectic temperature of LiF/$LiLuF_4$. The exothermic shoulders of the liquidus temperatures indicated that the eutectic composition of the LiF/$LiLuF_4$ system is approximately 78 mol%LiF + 22 mol%LuF_3, or $x = 0.22$. Undoped and Ce-doped LiF/$LiLuF_4$ eutectic composites with various x were solidified by the μ-PD method. According to XRD powder analysis, all the diffraction peaks of the undoped and Ce-doped eutectic solids corresponded to $LiLuF_4$ and LiF structures. The SEM images (obtained using BSE) of the cross-sectional cuts indicated the uniform eutectic areas that were composed of the rod-like single-phase fragments immersed into the matrix of other phase. On the other hand, the cluster phases with the dendrite structure were observed in the range of $x \geq 0.28$. The photoluminescence spectra had two emission peaks around 310 and 326 nm that originated from the 5d-4f transition of Ce^{3+}. The decay time of the emission at 326 nm was 32.3 ns.

Acknowledgement

This work was partially supported by the funding program for the next generation world-leading researchers, Japan Society for Promotion of Science.

References

1. Kim J, Cha BK, Bae JH, Lee C, Kim H, Chang S, et al. Fabrication and characterization of pixelated Gd_2O_2S:Tb scintillator screens for digital X-ray imaging applications. *Nucl Instrum Methods Phys Res Sect A* 2011;**633**:S303–5.
2. Nagarkar VV, Gupta TK, Miller SR, Klugerman Y, Squillante MR, Entine G. Structured CsI(Tl) scintillators for X-ray imaging applications. *IEEE Nucl Sci Trans* 1998;**45**(1):492–6.
3. Yasui N, Ohashi Y, Kobayashi T, Den T. Development of phase-separated scintillators with light-guiding properties. *Adv Mater* 2012;**24**:5464–9.
4. Lee JH, Yoshikawa A, Fukuda T, Waku Y. Growth and characterization of $Al_2O_3/Y_3Al_5O_{12}/ZrO_2$ ternary eutectic fibers. *J Cryst Growth* 2001;**231**(1–2):115–20.
5. Epelbaum BM, Yoshikawa A, Shimamura K, Fukuda T, Suzuki K, Waku Y. Microstructure of $Al_2O_3/Y_3Al_5O_{12}$ eutectic fibers grown by (-PD method. *J Cryst Growth* 1999;**198–199**(1):471–5.
6. Yokota Y, Chani V, Sato M, Tota K, Onodera K, Yanagida T, et al. Growth and crystallinity of shaped and multiple sapphire crystals by a micro-pulling-down method. *J Cryst Growth* 2011;**318**(1):983–6.
7. Yokota Y, Fujimoto Y, Yanagida T, Takahashi H, Yonetani M, Hayashi K, et al. Crystal growth of Na-Co-doped Ce:$LiCaAlF_6$ single crystals and their optical, scintillation, and physical properties. *Cryst Growth Des* 2011;**11**(11):4775–9.
8. Yokota Y, Kawaguchi N, Fukuda K, Yanagida T, Yoshikawa A, Nikl M. Development of modified micro-pulling-down method for bromide and chloride single crystals. *J Cryst Growth* 2011;**318**(1):908–11.
9. Yanagida T, Fujimoto Y, Kawaguchi N, Yokota Y, Kamada K, Totsuka D, et al. Scintillation properties of Ce-doped $LuLiF_4$ and $LuScBO_3$. *Nucl Instrum Methods Phys Res Sect A* 2011;**652**(1):251–5.
10. Thoma RE, Brunton GD, Penneman RA, Keenan TK. Equilibrium relations and crystal structure of lithium fluorolanthanate phases. *Inorg Chem* 1970;**9**(5):1096–101.
11. Harris IR, Safi H, Smith NA, Altunbas M, Cockayne B, Plant JG. The relationship between crystal growth behaviour and constitution in the systems LiF–LuF_3, LiF–ErF_3 and LiF–YF_3. *J Mater Sci* 1983;**18**:1235–43.
12. Santos IA, Klimm D, Baldochi SL, Ranieri IM. Experimental evaluation and thermodynamic assessment of the LiF–LuF_3 phase dagram. *Thermochim Acta* 2013;**552**:137–41.
13. Rambaldi P, Moncorge R, Wolf JP, Pedrini C, Gesland JY. Efficient and stable pulsed laser operation of Ce:$LiLuF_4$ around 308 nm. *Opt Commun* 1998;**146**:163–6.